Published as: Pedro H. Massinga Jr., Walter W. Focke, Olinto del Fabbro, Hans-Joachim Radusch. EVA nanocomposites based on South African Koppies clay. Journal of Vinyl and Additive Technology, 20(3) 2014, 143–151.

EVA nanocomposites based on South African Koppies clay

Pedro H. Massinga Jr.[#1], Walter W. Focke[*1], Ollinto del Fabbro[1], Hans-Joachim Radusch[2]

[1]Institute of Applied Materials, Department of Chemistry and Department of Chemical Engineering, University of Pretoria, Pretoria, South Africa
[2]Chair Polymer Technology, Martin Luther University Halle-Wittenberg, Halle (Saale), Germany

ABSTRACT

South African Koppies bentonite was organo-modified with single tail and double tail alkyl ammonium cationic surfactants with the latter intercalated both below and above the clay CEC. Corresponding poly(ethylene-co-vinylacetate) nanocomposites were prepared by twin-screw melt compounding. Transmission electron microscopy indicated the presence of mixed nano- and micron-sized clay morphologies. X-ray diffraction studies revealed that the crystallinity of the particles improved and that the d-spacing values increased on incorporating the clays in the polymer matrix. It is postulated that, rather than indicating polymer co-intercalation, this is caused by further intercalation of either excess surfactants or surfactant residues that were released by shear delamination of the clays during compounding. Improved mechanical properties were realized especially when using the clay containing the longer double tail surfactant intercalated at levels in excess of the cation exchange capacity of the clay. The nanocomposites showed improved tensile modulus and elongation at break values at the

[#]Present address: Universidade Eduardo Mondlane; Faculdade de Ciências; Campus Universitário Principal; Av. Julius Nyerere; P.O. Box 257; Maputo, Moçambique; E-mail: massingajr@uem.mz

[*]Corresponding author; e-mail: walter.focke@up.ac.za; phone: (+27) 12 420 3728; Fax: (+27) 12 420 2516

expense of a reduction in impact strength while tensile strength was about the same as for the neat polymer.

Keywords: Clay; nanocomposites; poly(ethylene-co-vinylacetate); exfoliation; intercalation.

INTRODUCTION

Smectite clays intercalated with alkylammonium cations [1] are widely used to prepared polymer nanocomposites [2-7]. These organoclays are functional polymer additives that enhance desirable material properties when dispersed as high aspect ratio particles in the polymer matrix [2-7]. This requires exfoliation (or at least significant delamination) of the clay platelets [8]. Full exfoliation of individual clay sheets is difficult to achieve in the absence of favorable interactions between the polar clays surfaces and the matrix polymer [3]. The compatibility of the clay and nonpolar polyolefin polymers such as polyethylene are improved by the organo-modification of the clay and by incorporating polar comonomers in the polymer structure [3,9-14]. Alexandre and Dubois [3] reported that no nanocomposites were formed when melt compounding organo-montmorillonite, functionalized with dimethyldioctadecylammonium, into high density polyethylene. However, partially intercalated and partially exfoliated morphologies were obtained with EVA copolymers even at low vinyl acetate content as low as 4.2 mol %. Therefore, ethylene-vinyl acetate (EVA) was chosen as the polymer matrix in this study.

Montmorillonite (MMT) is the base clay most often used to prepare organoclays. It features a layered structure comprising high aspect ratio negatively charged silicate sheets. Charge balancing cations such as Ca^{2+} or Na^{+}, often in hydrated form, are present in the interlayers [15]. Ion exchanging these cations with cationic surfactants (e.g., alkylammonium ions) yields organoclays. Since cationic surfactants are usually larger than the ions they

replace, their incorporation in the clay structure leads to an expansion of the interlayer spacing. Long-chain alkylammonium surfactants are preferred as they lead to greater separation of neighboring clay sheets and reduce the cohesive forces between them. Ultimately, this facilitates delamination of MMT particles in the polymer matrix [16]. The surfactants modification also lowers the surface energy of the sheets and wetting of the clay by the polymer matrix [6,17]. Thus surfactants act as compatibilizers between the hydrophilic clay and the hydrophobic polymer matrix [6].

Previous studies dealing with EVA-organoclay nanocomposites have considered the influence of various parameters on the degree of dispersion of the clay in the polymer matrix and the ultimate physical properties. These include, among others, the nature of the pristine clay [18-21], the clay organo-modifier [3,12,18, 21,22,23], the vinyl acetate content of the polymer [3,10,12,14,18,22-27], the processing techniques employed [25,28-31], and the presence of external compatibilizers [23,32,33]. Preparation of fully exfoliated EVA-layered silicate nanocomposites remains elusive. Most authors reported mixed morphologies comprising both intercalated tactoids and exfoliated sheets. Exfoliation was favored using EVA grades with higher vinyl acetate content [12]. Clays functionalized with alkyl substituent only were only partially exfoliated with the microstructure of the composites dominated by intercalated structures [12,21]. Nanocomposites based on a clay intercalated with methyl dihydroxyethyl hydrogenated tallow ammonium display the highest degree of exfoliation and clay stacking destruction, characterized by the absence of a characteristic XRD reflection [21]. Peeterbroeck et al. [21] speculate that this might be attributed to hydrogen bonding interactions between the hydroxyl groups on the surfactant and the ester functional groups of the EVA polymer chains. Surprisingly however, nanocomposites based on clays intercalated with dimethyldihydrogenated tallow ammonium provided better modulus improvements at comparable loadings despite the apparent limited clay exfoliation.

This suggests that well-dispersed clay tactoids comprising stacks of several clay sheets provide better reinforcement than fully exfoliated sheets. It would be interesting to determine whether a surfactant with only a single hydroxyethyl substituent will perform similarly to the one containing two. Furthermore, most studies employed clays with surfactants intercalated at approximately the cationic exchange capacity. However, intercalation can proceed to higher levels [1,34,35] and the effect of this on nanocomposite morphology and properties could be of interest. Consequently this study reports on the synthesis of organoclays based on Koppies bentonite from South Africa and the preparation and characterization of EVA-based clay nanocomposites. The effects of the structure of the surfactant (single tail with one polar 2-hydroxyethyl side group vs. two long-tail alkyl chains) and the degree of surfactant intercalation on the clay exfoliation behavior and the ultimate physical properties of the composites were investigated.

EXPERIMENTAL

Materials and Methods

Materials. Purified dry clay and soda ash activated bentonite slurry of Koppies clay, with a solids content of 18.9 wt. %, was supplied by G & W Base and Industrial Minerals (South Africa). The supplier stated a clay cation exchange capacity (CEC) of 85 meq/100 g dry clay according to the methylene blue method [36]. The clay was organo-modified by intercalation with cationic surfactants (Quats) using the procedures previously reported [37,38]. A Quat with a single long-tail plus one polar hydroxyethyl group as well as one with two long alkyl chains were utilized. Huntsman Surface Sciences UK supplied the single tail surfactant, lauryl dimethyl hydroxyethyl ammonium chloride (dodecyl[2-(2-hydroxyethoxy)ethyl]dimethylammonium chloride, CAS No. [94160-20-0]), as a 40 % aqueous solution under the trade name Empigen HBC 40. Ceca supplied the double tail

surfactant dihydrogenated tallow dimethyl ammonium chloride. It was a 76 % solution in a mixture of isopropanol and water, sold under the trade name M2SH-1. The alkyl chain distribution was stated as 64% saturated C18, 35% saturated C16 and 1% C18 chains containing a double bond.

EVA resin grade EV101 with 18 mol % vinyl acetate was supplied by APC (MFI 1.8 g/10 min at 190°C/2.16 kg; density 0.941 g/cm^3). The polymer was milled into a fine powder using a Pallmann 300 Series pulverizer.

Compounding and Injection Molding. EVA-organoclay masterbatches were prepared as follows. The EVA powder was mixed with organoclays powder in the mass ratio 4:1 and then compounded on a 28 mm co-rotating intermeshing twin-screw laboratory extruder (L/D = 16). The screw design comprised intermeshing kneader elements with a forward transport action. The barrel temperature profile ranged from 170 ºC to 180 °C and the screw speed was 168 rpm. The extruded masterbatch strand was dried, granulated and then pulverized. This powder was let down in virgin resin in order to set the required final clay content (loading levels up to 6.5 wt. % targeted). It was compounded twice at the same conditions in order to ensure a good dispersion of delaminated clay platelets. Following each compounding step, the extruded strands was granulated and dried. Test bars, conforming to ASTM D638, were injection molded on an Engel 3040 injection-molding machine. Barrel temperatures varied from 170 °C to 180 °C for all samples. The injection and holding pressures were 180 bar and 80 bar respectively. The injection speed was 6 mm/s, the stroke was 22 mm and the clamping force 350 kN.

Characterization

Thermogravimetric Analysis. Thermal behavior under oxidative conditions was investigated on a Mettler Toledo A851 instrument. About 17 mg powder was placed in open

70 μL alumina pans. The sample was heated from 25 to 1000 °C at a scan rate of 10 °C/min with air flowing at a rate of 50 mL/min.

X-ray diffraction. Wide-angle powder X-ray diffraction (WAXS) experiments were performed on a PANalytical X-pert Pro diffractometer. The instrument featured variable divergence and receiving slits and an X'celerator detector using Fe filtered Co Kα radiation (λ = 0.17901 nm). X'Pert High Score Plus software was used for data reduction.

Electron Microscopy. Samples were cryo-sectioned with a diamond knife at a temperature below -110 °C on a Lecia-Riechert Ultracut R instrument with an EMFCS cryo attachment. The nominal sectioning thickness was 90 ± 10 nm. Each sample was mounted on a 300 mesh copper/palladium grid and viewed on a JEOL 2100F TEM using an acceleration voltage of 200kV.

Tensile and Impact testing. A Lloyds Instruments LRX machine was used for tensile testing (ASTM D638-M) at the cross-head speed of 50 mm/min. The tensile impact tests were done on a Zwick Impact Tester.

Rheometry. The rheological properties were determined in oscillatory mode at 170 ºC. An Advanced Rheometer AR 2000 (TA Instruments) was used. The cone-and-plate geometry was chosen to ensure a uniform the shear rates across the sample. The diameter of the disc was 25 mm, the gap was set at 54 μm and the strain amplitude as set at 1%.

Dynamic Mechanical Analysis. Visco-elastic behavior was studied on an Eplexor 500 N Qualimeter dynamic mechanical analyzer (DMA) from Gabo. The storage modulus (E'), loss modulus (E") and tan δ were determined as a function of temperature at a frequency of 1 Hz in tensile mode. The static load was 2.5 MPa with 2% maximum strain or 1.75 MPa with a maximum strain of 0.6%. The samples were heated from -60 °C to 60 °C at a scan rate of 1 °C/min.

RESULTS

Massinga *et al.* [37] and Massinga and Focke [38] provide more detailed information on the characterization for the present, as well as some other organoclays. FTIR data can establish whether the surfactants indeed intercalated and allow one to probe the state of the chains in the clay galleries. Figure 1 shows the FTIR spectra for the neat Koppies clay as well as two

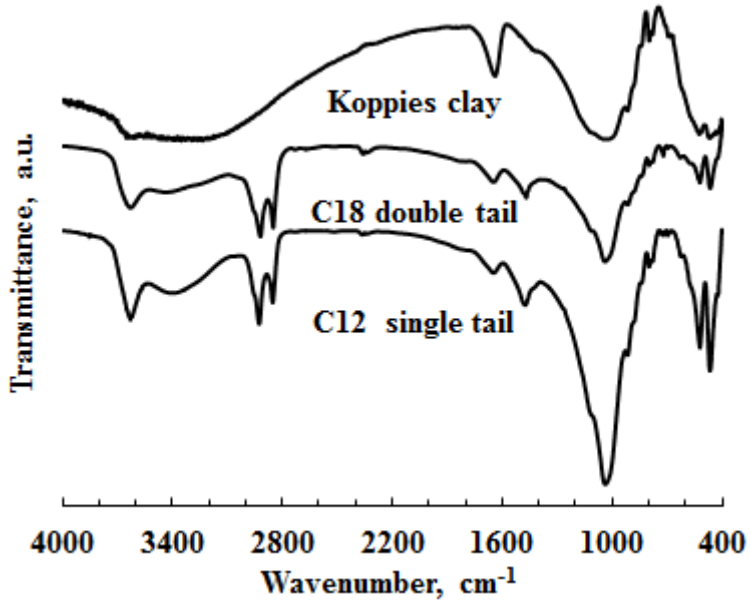

Figure 1. FTIR spectra for Koppies clay and organoclays

organoclays. The spectra for the organoclays featured strong bands near 2920 cm^{-1} and 2850 cm^{-1}. These arise from the CH_2 asymmetric $\upsilon_{as}(CH_2)$, and symmetric $\upsilon_s(CH_2)$ stretch modes, respectively. The presence of these bands provides evidence for the presence of the surfactants in the organoclays. Vaia *et al.* [39] proposed the use of the $\upsilon_{as}(CH_2)$ band to probe the nature of the interlayer structure. The wavenumber and the width of this band are sensitive to the gauche/trans conformer ratio and the packing density of the chain methylenes. It varies from ca. 2918 cm^{-1} for the methylene chains in the all-trans ordered arrangement in a crystalline state to 2929 cm^{-1} when the chains are in a liquid-like state [39,40]. The peak positions of the methylene asymmetric bands found for the present organoclays were 2926

cm^{-1} and 2922 cm^{-1} for the C12 single tail and the C18 double tail surfactant samples respectively. These values are located in the middle of the range suggesting that the intercalated chains adopted a disordered, liquid-like structure.

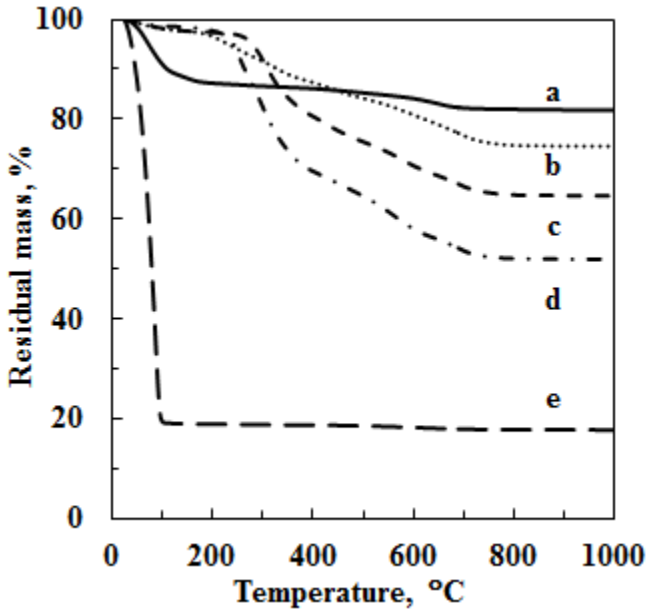

Figure 2. Thermo-gravimetric analysis of neat Koppies clay, the soda ash activated bentonite slurry and the organoclays. a. Koppies bentonite; b. C12 single tail at CEC; c. C18 double tail at CEC; d. C18 double tail at 1.5 CEC, and e. Bentonite slurry.

Figure 2 shows the thermogravimetric analysis of the clays and the organoclays heated in an air atmosphere. The surfactant loading of the organoclays was determined from the residual masses determined at 150 °C and 1000 °C and are reported in Table 1. The clay prepared with an excess of C18 double tail surfactant contained 143 meq/100 g dry clay. This exceeds the cationic exchange capacity (CEC) of the clay and is almost twice the amount of surfactant present in the other two organoclays samples (mole basis). Note that despite repeated attempts, using excess surfactant did not lead to higher clay intercalation levels for the C12 single tail surfactant.

Table 1. Thermogravimetric analysis of neat clay, bentonite slurry and organoclays in air

Sample/surfactant intercalated	Residual mass at		Organic content
	1000°C	150°C	meq/100 g clay
Bentonite slurry	17.71	18.95	-
Koppies bentonite	82.29	88.22	-
C12 single chain	74.57	97.58	74
C18 double chain	64.65	97.66	76
C18 double chain (excess)	51.93	98.41	143

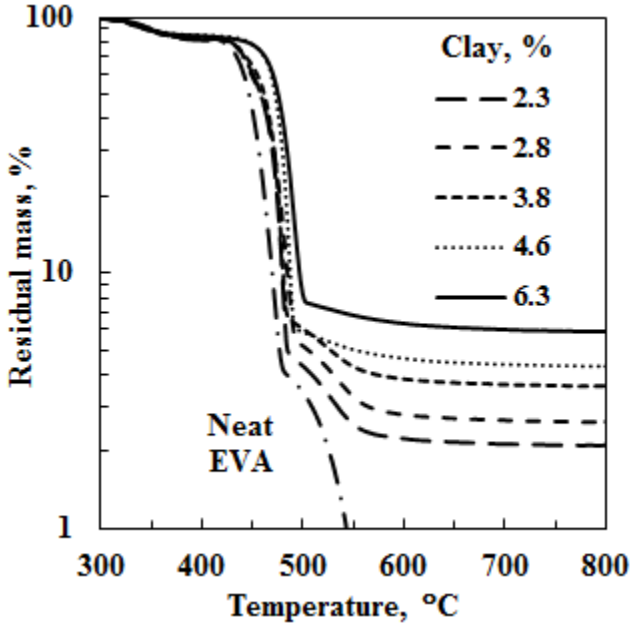

Figure 3. Thermo-gravimetric analysis of neat EVA and EVA-clay composites based on the organoclays prepared with a stoichiometric amount of the C18 double tail surfactant. Similar TGA traces were obtained with the other EVA-clay composites.

Figure 3 shows representative TGA results for EVA-organoclay composites. Up to a temperature of about 400 °C, all samples showed a similar mass loss profile. Thereafter the observed mass loss was less for the samples with higher clay loadings. At high temperatures, the mass loss reached a plateau value corresponding to the calcined clay residue. This allowed the estimation of the actual clay content of the EVA composites from the residual mass observed at 1000 °C. Table 2 reports the TGA-determined dry (inorganic) clay contents of the EVA-organoclay composites.

Table 2. Clay content from TGA and mechanical properties of EVA-clay composites

EVA composite	Clay wt. %	Tensile Strength, MPa		Strain at break, %		Young's modulus, MPa		Tensile impact, MJ/m^2	
Neat EVA	0.0	9.1	0.3	287	18	24.3	2.2	0.57	0.01
C12 single chain	2.7	9.0	0.2	250	14	34.1	2.4	0.41	0.06
(SC12)	3.2	9.2	0.2	236	10	37.7	3.7	0.41	0.02
	4.5	9.3	0.2	245	12	33.1	2.6	0.39	0.02
C18 double chain	2.8	9.3	0.2	271	11	39.2	3.0	0.39	0.03
	3.9	9.4	0.3	274	19	37.3	2.9	0.40	0.02
DC18<CEC	4.6	9.3	0.2	274	7	42.3	2.5	0.45	0.03
	6.3	9.5	0.2	284	8	49.3	4.3	0.37	0.02
C18 double chain	3.1	12.4	0.3	445	19	38.1	1.5	0.40	0.03
(excess surfactant)	4.7	16.2	0.2	721	22	48.9	2.3	0.35	0.01
(DC>CEC)	6.6	15.1	0.3	663	11	73.1	4.6	0.36	0.03

Note: Second number in each column indicates standard deviation in measured value

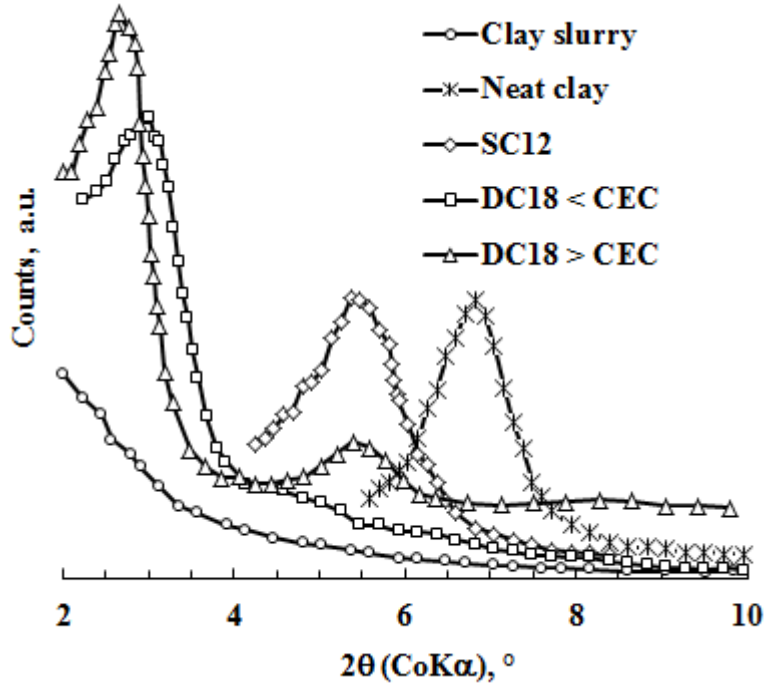

Figure 4. XRD diffractograms for the neat clay, the soda ash activated clay slurry and the organobentonites.

Figure 4 presents the XRD diffractograms for the neat bentonite clay, the soda ash activated clay slurry and the organic derivatives. The diffractogram of the neat clay slurry is featureless indicating that the bentonite particles were present in an exfoliated form. The basal reflection observed at $2\theta = 6.76^{o}$ for neat bentonite corresponds to $d_{001} = 1.52$ nm. This

falls within the 1.2-1.6 nm range typical for smectite minerals under ambient temperature and humidity conditions [41].

The chain length, surfactant loading and configurations the surfactant molecules assume in the interlayer, determine the basal spacing of organoclays [1]. The surfactant cations are electrostatically "attached" to the clay surfaces with the alkyl chains preferring to tightly pack together in order to maximize van der Waals interactions. Excess surfactant probably intercalated in the neutral salt form together with (hydrated) counter ions [1,35]. The diffractograms for the organoclays showed reflections at lower 2θ values confirming the intercalation of the surfactants. The observed XRD d-spacing for the single tail surfactant organoclay sample was 1.92 nm. As previously reported [37,38], this value is consistent with interdigitated monolayer surfactant intercalation of the C12 single tail surfactant (SC12). As mentioned before, samples prepared in the presence of excess of C12 surfactant featured a nearly identical XRD diffractogram and surfactant content. The XRD-estimated d-spacings were 3.56 nm and 3.77 nm for the organoclay samples prepared with stoichiometric amount (DC18 < CEC) and with an excess of the C18 double tail (DC18 > CEC) surfactant respectively. These values are consistent with bilayer surfactant intercalation. The additional reflection at 5.45°, in the diffractogram for the DC18 > CEC sample, corresponds to a second order basal reflection. This second reflection was not observed for the DC18 < CEC sample suggesting that more ordered intercalation occurred in the former case.

In contrast to those for the EVA-clay composites based on the C18 double tail surfactant, The XRD diffractograms for EVA composites based on the C12 single tail surfactant did not show well-defined reflections. See Figure 5a. Figure 5b shows XRD diffractograms for the DC18 > CEC organoclays and the corresponding EVA composite containing 4.7 wt. % clay. The diffractogram for all the EVA composites with organoclays based on the C18 double tail surfactant were virtually identical irrespective of the clay

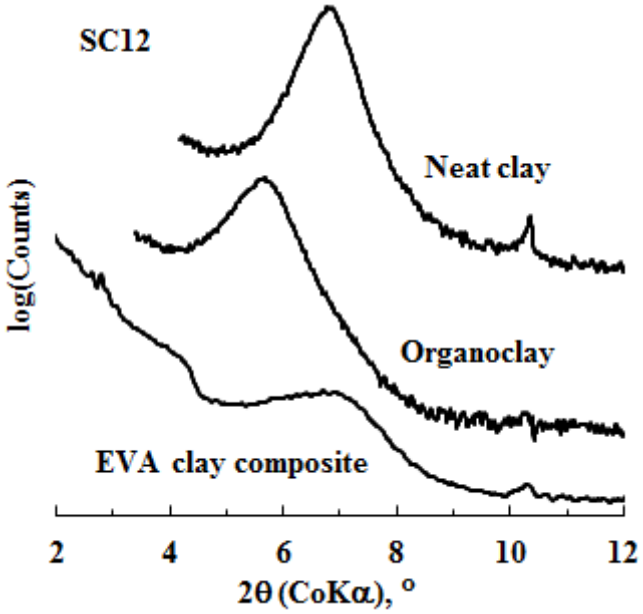

Figure 5a. XRD diffractograms for the SC12 single tail organoclay and its corresponding EVA composite containing 4.5 wt. % bentonite (inorganic content).

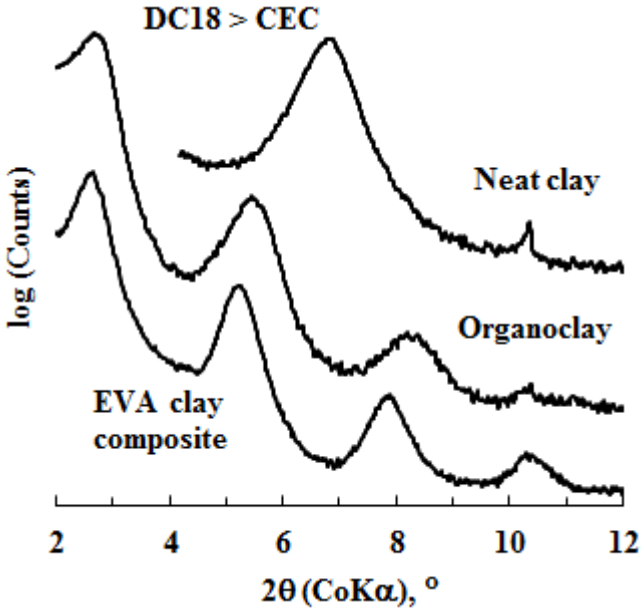

Figure 5b. XRD diffractograms for the C18 double tail organoclay, prepared with an excess of surfactant (DC18 > CEC), and its corresponding EVA composite containing 4.7 wt. % bentonite (inorganic content).

loading. They all showed four clear reflections associated with an integral series of basal plane reflections. This indicates a homogeneous distribution of the alkylammonium cations in the MMT interlayers [35]. Compared to the organoclays, the reflections are sharper and their

position shifted to lower 2θ values. This implies an increase in perfection and an expansion of the clay gallery height to effect a d-spacing as high as 3.9 nm.

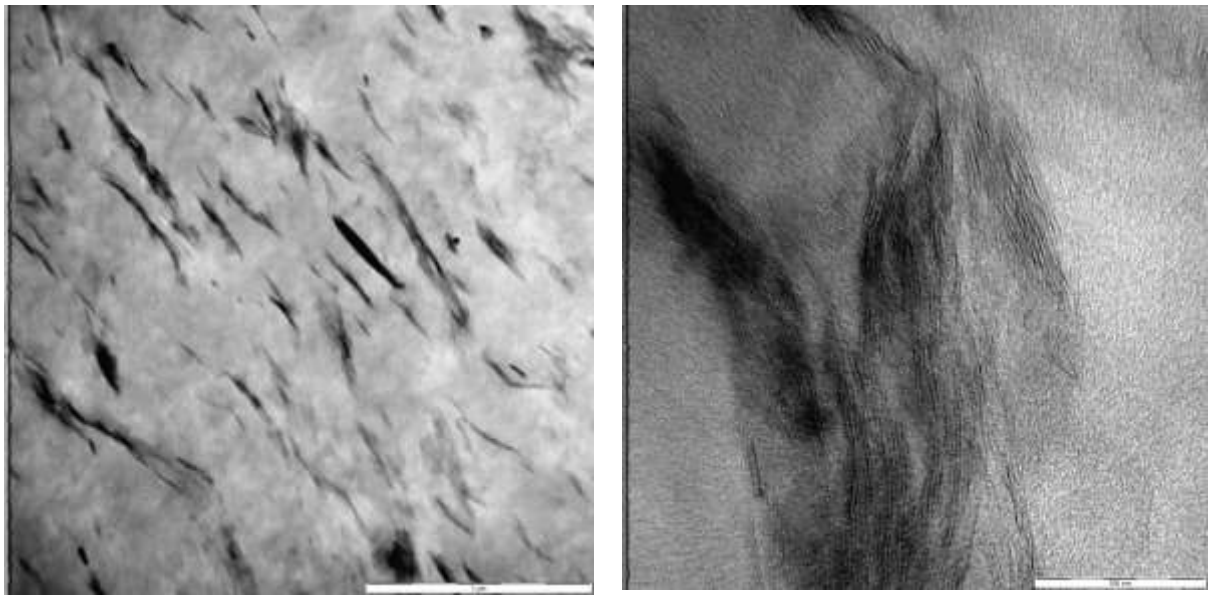

A **B**

Figure 6. Representative TEM micrographs of the DC18 > CEC-based EVA-organoclay composite containing 4.7 wt.% inorganic clay. The white scale bar corresponds to 1 μm and 100 nm in (A) and (B) respectively.

Figure 6 shows TEM pictures for the DC18 > CEC-based EVA-organoclay composite containing approximately 4.7 wt. % inorganic clay. Small clay particles are visible at the micron scale but extensive delamination is evident in pictures with nanoscale resolution. Similar observations were made for the other organoclay composites. This implies that the EVA-organoclay compounds prepared in the present study were a combination of micro- and nanocomposites. The flake-like clay particles seen in composites based on the single tail surfactant were significantly smaller and thinner than the ones observed in the two composites comprising double tail surfactant. It seems reasonable to conclude that a surfactant with a single hydroxyethyl substituent facilitates clay sheet dispersions particularly well, similarly to those containing two hydroxyethyl substituents, when all other characteristics are similar.

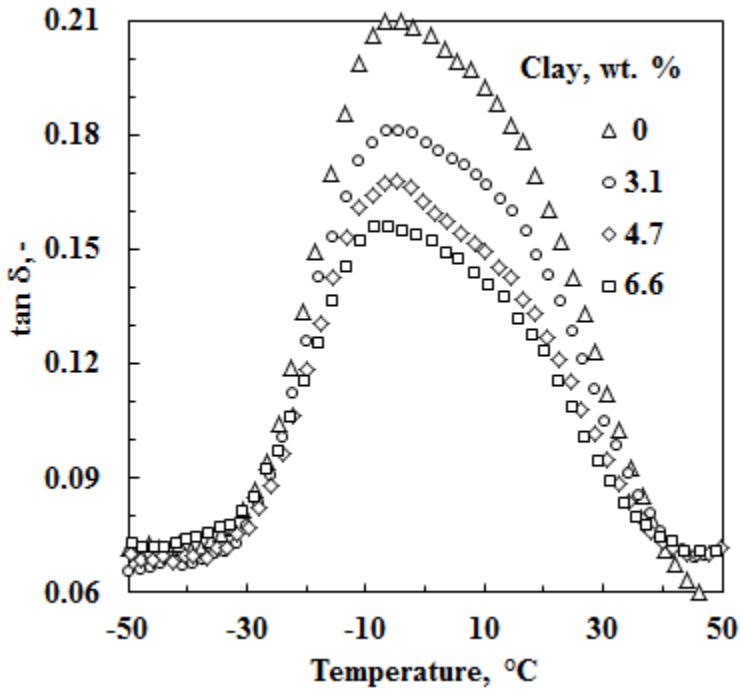

Figure 7. Effect of clay loading on tan δ for EVA-organoclay composites based on the clay containing double tail surfactant intercalated in excess of the clay CEC.

Figure 7 shows tan δ as a function of temperature and clay concentration for the composite based on the clay containing double tail surfactant intercalated in excess of the clay CEC. The shape of the tan δ curve remains approximately the same but the peak height decreased with increase in clay content. The tan δ curves for the composites made with the other two organoclays showed similar behavior. The peak in this curve can be associated with the glass transition temperature and it was about -7 °C for the neat EVA as well as for all the composites. This suggests that the presence of the clay did not significantly affect the mobility of the polymer chains of the matrix.

Table 2 reports tensile and tensile impact properties for the EVA nanocomposites. The tensile impact strength decreased with clay loading for all samples. Adding clay reduced it by values between 21 % and 38 %, depending on the clay used. For the SC12 and DC18 < CEC composites, tensile strength increases marginally and strain at break decreases slightly

with increase in clay content. In contrast, the SC18 > CEC composites showed significant improvements in both tensile strength and ultimate elongation. Optimum results were obtained for the compound with intermediate clay content (4.7 wt. % clay). In this case, the tensile strength and ultimate elongation were 78 % and 151 % higher than the corresponding values for the neat polymer.

Table 2 also summarizes the tensile modulus data obtained from tensile tests. The composites differed markedly with respect to the increase in the Young's modulus. The composite based on the clay containing double tail surfactant intercalated in excess of the CEC showed the best performance. The modulus was three times higher than that of the neat EVA at a loading of 6.6 wt. %. At a similar clay content, the composite prepared using the organoclay loaded with the same surfactant but at the lower level, provided only a doubling the modulus. Table 2 also shows that the increase in modulus with increasing clay content was less for the composites based on the single long-tail alkyl chain surfactant. Figure 8

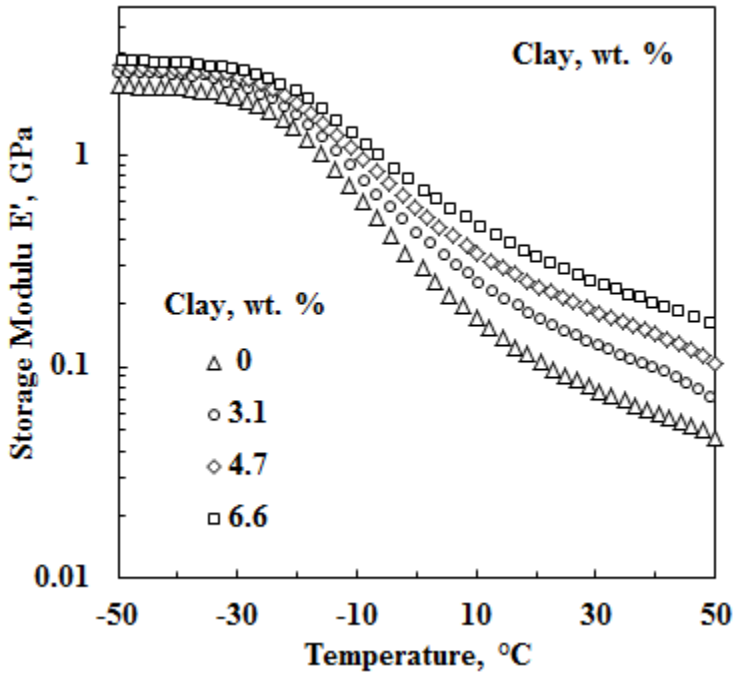

Figure 8. DMA-determined storage modulus as a function of temperature and clay concentration for EVA-organoclay composites based on the clay containing double tail surfactant intercalated in excess of the clay CEC.

shows the DMA-determined storage modulus as a function of temperature and clay concentration for the EVA-organoclay composite based on the clay containing double tail surfactant intercalated in excess of the clay CEC. It shows that the stiffness enhancement is limited at low temperatures where the polymer is in a glassy state and more pronounced in the temperature range corresponding to the rubbery plateau, i.e. above the glass transition temperature. The other EVA-organoclay composites showed similar behavior. Figure 9 compares the modulus enhancement E'_c/E'_p found for the composites containing

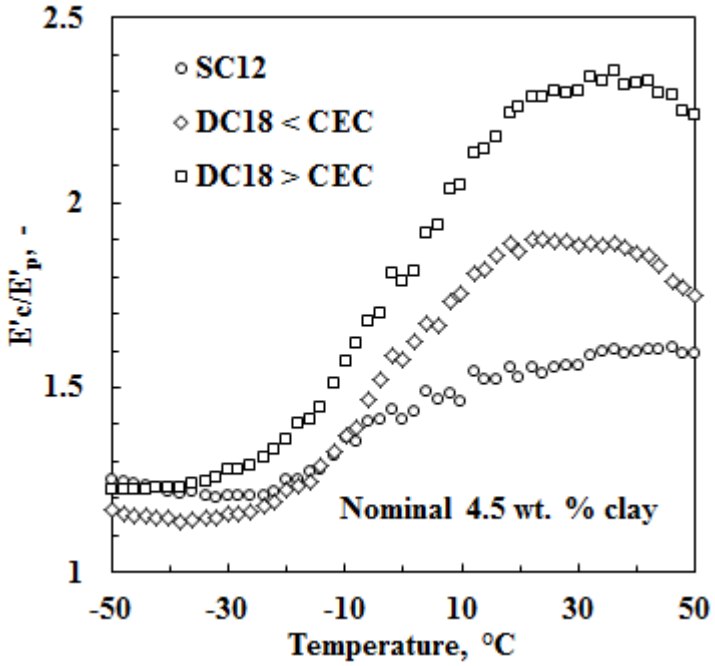

Figure 9. Comparison of the modulus enhancement (E'_c/E'_p) found for the composites containing approximately 4.5 wt. % clay**.**

approximately 4.5 wt. % clay. The main difference was that the modulus enhancement was less. Figure 8 and Figure 9 confirm that the modulus enhancement trends observed with tensile testing hold over the full temperature range. They show that the enhancement achieved in the glassy region is small and similar for the different organoclays composites but that it becomes differentiated at elevated temperatures.

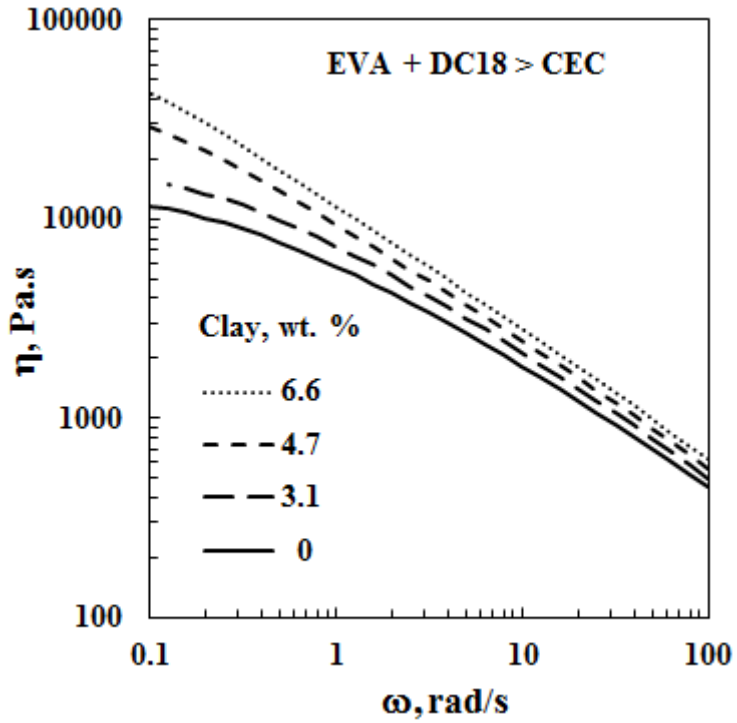

Figure 10. Rheology curves obtained at 170 °C showing the effect of clay content and shear rate on the melt viscosity of EVA-clay composites containing the clay prepared with excess double tail surfactant.

The rheological behavior of molten polymer nanocomposites complements XRD and TEM information on the degree of exfoliation of clay platelets in a polymer matrix [26]. Figure 10 shows the effect of clay content and shear rate on the melt viscosity of EVA-clay composites containing the clay prepared with excess double tail surfactant. The high viscosity at low shear rates points to strong interactions between the delaminated clay platelets and the polymer chains or, alternatively, the formation of network structures by clay particle interactions. Pronounced shear thinning indicates extensive clay exfoliation in a given system [26,42,43]. The nanocomposites internal structure is retained at low shear rates but at high shear rates the clay network structures break down and the platelets tend to orient in the flow direction. The resulting platelet alignment decreases the apparent viscosity so that it approaches that of the neat polymer melt [42,43].

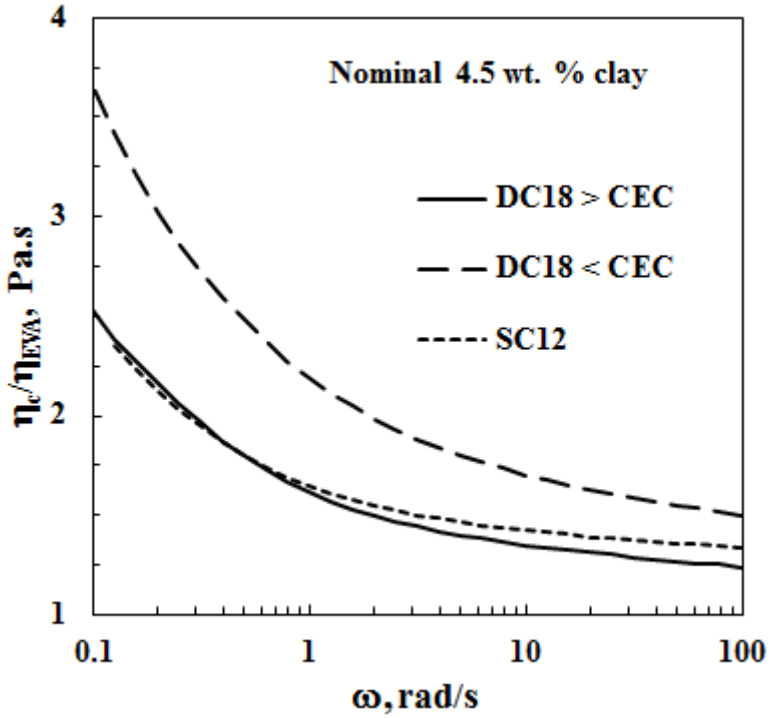

Figure 11. Comparison of the relative viscosities (measured at 170 °C) of composites scaled with respect to that of the neat EVA at a clay content of ca. 4.5 wt. %.

The other EVA-clay composites showed similar behavior. Figure 11 compares the relative viscosities scaled with respect to that of the neat EVA at a clay content of ca. 4.5 wt. %. Interestingly, the highest melt viscosity is shown by the DC18 < CEC sample. The melt viscosities of the other two clay composites were similar but significantly lower.

DISCUSSION

The final properties of clay-based nanocomposites are determined by their morphology. Homogeneous dispersion of large numbers of stiff high-aspect ratio platelets in the polymer matrix is usually the desired outcome. This implies the need for extensive delamination and/or exfoliation of the clay particles during the preparation step. Factors that control this process include the properties of the matrix and the organoclays, and the processing route used. Surfactant structural issues significantly affect organoclays properties and ultimately

the nanocomposite morphology [8]. This study held the montmorillonite clay base, the polymer matrix and the melt processing technique constant and focused on the effect of the surfactant structure and its loading in the organoclay. Fornes et al. [8] studied Nylon 6 composites and observed that decreasing the number of long alkyl tails from two to one, and using an equivalent amount of surfactant with the montmorillonite (as opposed to adding excess) led to greater extents of silicate platelet exfoliation, increased moduli, higher yield strengths, and lower values for the elongation at break. This study found that the opposite holds for EVA-based micro-nanocomposites prepared by melt compounding. The present results are in better agreement with the findings of Shah et al. [16] for nanocomposites from poly(ethylene-co-methacrylic acid) copolymers. In these systems four distinct surfactant structural effects lead to improved levels of delamination/exfoliation and higher stiffness for these nanocomposites. They are higher number of alkyl tails on the amine rather than one, longer alkyl tails instead of shorter ones, use of 2-hydroxyethyl groups as opposed to methyl groups on the ammonium ion, and an excess amount of the amine surfactant on the clay instead of an equivalent amount [16].

We pose the following tentative rationalization for the results presented in this communication. XRD results indicated interdigitated monolayer intercalation of the single-tail surfactant in the clay while the double tail surfactant intercalated in a double layer fashion [37,38]. Basal spacing values of the neat organoclays were readily determined as the XRD diffractograms showed clear basal reflections. Incorporating the clays into the EVA by melt compounding changed these diffractograms dramatically. The XRD diffractograms of the SC12-based nanocomposites became almost featureless suggesting extensive disruption of the regular clay platelet stacking. Just hints of poorly resolved reflections remained. Such a drastic change is consistent with extensive clay delamination that reduces the remaining platelets to stacks comprising few clay sheets. TEM provided some evidence for this

possibility. An alternative possibility is a significant increase in the degree of disorder in the stacking of the platelets within the tactoids. Random co-intercalation of EVA polymer chains can result in such a severe disruption in the regularity of sheet stacking. The presence of a single hydroxyethyl substituent on the C12 surfactant appears sufficient to encourage co-intercalation of the EVA chains as it is capable of hydrogen bonding with the ester functional groups.

In contrast, the XRD diffractograms for the nanocomposites made using the double tail surfactant showed sharpened reflections and, in some instances, the emergence of additional reflections attributable to multiple basal reflections. This is consistent with an increase in the structural order of the tactoids due to improved packing of the surfactants intercalated in the clay galleries. It is significant that the diffractograms, and thus the basal spacings, were virtually identical irrespective of the amount of surfactant employed in the synthesis of the organoclays. Alexandre and Dubois [3] previously noted an increase in the basal spacing of double tail intercalated MMT when incorporated into EVA. They also found that the surfactant intercalated into the neat clay when both were individually dispersed in molten EVA [22]. An increase in basal spacing has also been observed in other polymer matrices [6] and it is generally taken as evidence that polymer intercalated into the clay galleries has occurred [44]. However, the observed sharpening of the reflection peaks observed presently is in our opinion not consistent with polymer intercalation into the clay galleries. Since the polymer chains vary in length and in composition, one would expect significant variations in d-spacing values and thus a broadening of the XRD reflections if they were co-intercalated. This is in fact observed with the clay intercalated with surfactant containing the hydroxyethyl substituent. The common shift to lower Bragg angles implies that, more likely, the EVA chains did not enter the clay galleries. Instead, it seems more probable that “surplus” surfactant molecules released by the delamination and dispersion of

the clay sheets during compounding were taken up in the remaining tactoids resulting in improved ordering through tighter packing of the alkyl chains in the galleries. Nevertheless, it should be kept in mind that the XRD traces only capture the thicker tactoids and certainly not the well dispersed single (exfoliated) clay sheets.

The consequence of delamination and exfoliation of clay particles manifests itself primarily in the enhancement of the viscosity of the liquid melt and the modulus in the solid state. Two main mechanisms operate to increase the modulus of composites comprising well-dispersed clay platelets [6]. The clay platelets particles are significantly stiffer than the polymer matrix. Thus, the first effect derives from their load carrying ability. Additionally, an apparent matrix stiffness increase arises from the tendency of the clay surfaces to constrain the motion of adjacent polymer chains. Strong polymer chain-clay surface interactions strengthen this confinement effect. Both mechanisms benefit from an increase in the degree of clay exfoliation as the interfacial area also increases.

Table 2 and Figure 9 compare moduli for the composites at comparable clay contents. It is clear that the composites based on the double tail modified clays performed better at modulus enhancement than the single tail surfactant modified clay especially when intercalation beyond a CEC excess was achieved. This despite the fact that the single tail surfactant is probably is more likely to interact with the EVA chains as discussed above. Thus it may be easier to exfoliate bilayer-intercalated clay than interdigitated monolayer intercalated clay. The increase in the melt viscosities mirrored the modulus enhancement for the composites based on the two clays prepared with an equivalent amount of surfactant. Surprisingly this was not the case for the composite based on an excess of the DC18 surfactant. It provided the best performance in modulus improvement but featured a lower viscosity than the DC18 < CEC sample. The lowering of the viscosity of the DC18 > CEC composites was unexpected. However, this can be explained by assuming that some of the

excess surfactant must have de-intercalated and that these molecular surfactant molecules imparted an external lubrication effect.

Finally, the nanocomposites displayed a large increase in the elongation at break. This could be due to the plasticizing effect of the galleries, their contribution to the formation of dangling chains and conformational effects at the clay-matrix interface [7].

CONCLUSIONS

Single tail C12 with a hydroxyethyl substituent and double tail C18 alkyl ammonium cationic surfactants were effectively intercalated into South African Koppies bentonite. In the latter case intercalation levels both below and above the clay CEC were achieved. XRD results were consistent with interdigitated single layer and double layer intercalation for the C12 and C18 organoclays respectively. TEM and XRD revealed that EVA nanocomposites prepared by twin-screw melt compounding showed mixed exfoliated/intercalated microstructures. Samples prepared using the clay intercalated with a double tail surfactant in excess of its CEC gave the better improvement in Young's modulus while showing a lower viscosity enhancement. It is postulated that it was easier to delaminate this bilayer-intercalated clays and that excess surfactant acted as an external lubricant thereby reducing the apparent melt viscosity.

Acknowledgements

Financial support for this research from the Institutional Research Development Programme (IRDP), the South Africa/Mozambique Collaborative Programme of the National Research Foundation (NRF), and the Mozambican Research Foundation (FNI) are gratefully acknowledged. We are also grateful for samples and technical support provided by G & W

Base & Industrial Minerals. The authors also acknowledge technical support from Dr. Wurtzler, Ms. Kamper, Mr. Allan Hall and Mr. Chris Van der Merwe.

REFERENCES

1. G. Lagaly, *Solid State Ionics*, **22**, 43–51 (1986).
2. P. LeBaron, Z. Wang, and T. Pinnavaia, *Appl. Clay Sci.*, **15**, 11–29 (1999).
3. M. Alexandre, and P. Dubois, *Mat. Sci. Eng*., **28**, 1–63 (2000).
4. S. Sinha Ray, and M. Okamoto, *Prog. Polym. Sci*., **28**, 1539–1641 (2003).
5. D.R. Paul, and L.M. Robeson, *Polymer*, **49**, 3187–3204 (2008).
6. S. Pavlidou, and C. Papaspyrides, *Prog. Polym. Sci*., **33**, 1119–1198 (2008).
7. P.H.C. Camargo, K.G. Satyanarayana, and F. Wypych, *Mat. Res*., **12**(1) *São Carlos* (2009).
8. T. Fornes, P. Yoon, D. Hunter, H. Keskkula, and D.R. Paul, *Polymer*, **43**, 5915–5933 (2002).
9. F.P. La Mantia, S. Lo Verso, and N. Tzankova Dintcheva, *Macromol. Mater. Eng*., **287**, 909 (2002).
10. F. Cser, and S.N. Bhattacharya, *J. Appl. Polym. Sci*., **90**, 3026–3031 (2003).
11. J. Zhang, and C.A. Wilkie, *Polym. Degrad. Stabil*., **80**, 163–169 (2003).
12. W. Zhang, D. Chen, Q. Zhao, and Y. Fang, *Polymer*, **44**, 7953–7961(2003).
13. Y. Tang, Y. Hu, J. Wang, R. Zong, Z. Gui, and Z. Chen, Y. Zhuang, and W. Fan, *J. Appl. Polym. Sci*., **91**, 2416–2421 (2004)
14. L. Cui, X. Ma, and D. Paul, *Polymer*, **48**, 6325–6339. (2007).
15. A. Rehab, and N. Salahuddin, *Mat. Sci. Eng. A*, **399**, 368–376 (2005).
16. R. Shah, D. Hunter, and D. Paul, *Polymer* **46**, 2646–2662 (2005).

17. E.P. Giannelis, *Appl. Clay. Sci*., **15**, 1–9 (1999).

18. M. Zanetti, G. Camino, R. Thomann, and R. Mülhaupt, *Polymer*, **42**, 4501–4507 (2001).

19. A. Riva, M. Zanetti, M. Braglia, G. Camino, and L. Falqui, *Polym. Degrad. Stabil*., **77**, 299–304 (2002).

20. M.C. Costache, D.D. Jiang, C.A. Wilkie, *Polymer*, **46**, 6947–6958 (2005).

21. S. Peeterbroeck, M. Alexandre, R. Jérôme, and P. Dubois, *Polym. Degrad. Stabil*., **90**, 288–294 (2005).

22. M. Alexandre, G. Beyer, C. Henrist, R. Cloots, A. Rulmont, R. Jéróme, and P. Dubois, *Chem. Mater*., 13, 3830–3832 (2001)

23. C.H. Jeon, S.H. Ryu, and Y.-W. Chang, *Polym. Int*., **52**, 53–157 (2003).

24. V. Pasanovic-Zujo, R.K. Gupta, and S.N. Bhattacharya, *Rheol. Acta*, **43**, 99–108 (2004).

25. F. Zhang, and U. Sundararaj, *Polym. Compos*., **25**, 535–542 (2004).

26. R. Gupta, V. Pasanovic-Zujo, and S. Bhattacharya, *J. Non-Newtonian Fluid Mech*., **128**, 116–125 (2005).

27. J. Marini, M.C. Branciforti, and C. Lotti, *Polym. Adv. Technol*., **21**, 408–417 (2010).

28. D.S. Chaudhary, R. Prasad, R.K. Gupta, and S.N. Bhattacharya, *Polym. Eng. Sci*., 898–897 (2005).

29. D.S. Chaudhary, R. Prasad, R.K. Gupta, and S.N. Bhattacharya, *Thermochim. Acta*, **433**, 187–195 (2005).

30. F.P. La Mantia, and N. Tzankova Dintcheva, *Polym. Test.*, **25**, 701–708 (2006).

31. V. Pistor, A. Lizot, R. Fiorio, and A.J. Zattera, *Polymer*, **51**, 5165–5171 (2010).

32. I.S. Suh, S.H. Ryu, J.H. Bae, and Y.W. Chang, *J. Appl. Polym. Sci.*, **94**, 1057–1061 (2004).

33. C. Martins, N. Larocca, D. Paul, and L. Pessan, *Polymer*, 50, 1743–1754 (2009).

34. S. Xu, and S.A. Boyd, *Langmuir*, **11**, 2508–2514 (1995).

35. Z. Klapyta, T. Fujita, and N. Iyi, *Appl. Clay Sci.*, **19**, 5–10 (2001).

36. P. Huang, and G. Brindley, *Clays Clay Miner*., **18**, 203–212 (1970).

37. P. Massinga Jr., W.W. Focke, P. de Vaal, and M. Atanasova, *Appl. Clay Sci*., **49**, 142–148 (2010).

38. P. Massinga Jr., and W.W. Focke, *Mol. Cryst. Liq. Cryst*., **555**, 85–93 (2012).

39. R. Vaia, R. Teukolsky, and E. Giannelis, *Chem. Mater*., **6**, 1017–1022 (1994).

40. H. Hongping, F. Ray, and Z. Jianxi, *Spectrochim. Acta*, **60**, 2853–2859 (2004).

41. L.A. Utracki, *Clay–containing polymeric nanocomposites*, Vol. 1, Rapra Technology Limited, UK (2004).

42. R. Wagener, and T. Reisinger, *Polymer*, **44**, 7513–7518 (2003).

43. A. Szép, A. Szabó, N. Tóth, P. Anna, and G. Marosi, Role of montmorillonite in flame retardancy of ethylene-vinyl acetate copolymer, *Polym. Deg. Stabil.*, **91**, 593–599 (2006).

44. G. Beyer, Nanocomposites: a new class of flame retardants for polymers, *Plast. Addit. Compound.*, **4**, 22–27 (2002).